https://doi.org/10.5194/egusphere-2026-1999
Preprint. Discussion started: 29 May 2026

Evolution of the Unsaturated Permeability and Internal Erosion Characteristics of Ili loess under Rainfall

Abuduwaresi Tuerxun[1]&Kaidierding Wulamu[2], Zizhao Zhang[1,3*], Qianli Lv[1], Runsen Lai[1,3], Yanyang Zhang[1,3], Zhiguo Xu[4]

[1] School of Geology and Mining Engineering, Xinjiang University, Urumqi 830017, China
[2] Emergency Management Bureau of Yining City, Yining 835000, China
[3] Research Base of National Key Laboratory for Intelligent Construction and Healthy Operation and Maintenance of Deep Earth Engineering, Xinjiang University, Urumqi 830017, China
[4] Xinjiang Geological Bureau Hydrogeology and Environmental Geology Survey Center, Urumqi 830017, China
*Correspondence: zhangzizhao@xju.edu.cn; Tel.: +86-136-3997-7295

Abstract: The evolution of microcharacteristics of the loess affected by the combination of permeability and seepage erosion has a significant impact on the integrity and stability of the loess slopes. To investigate the in-behind mechanics of the loess under rainfall, the self-designed experimental framework was adopted for laboratory procedures, during which scanning electron microscope tests, laser particle size analysis, and numerical simulation analysis were conducted concurrently. The experimental results showed that the unsaturated permeability of the loess increases exponentially with increasing water content. The migration of clay particles alters soil microstructure, thereby enhancing porosity and permeability, which is associated with significant clay particle loss within the shallow layer. Loess accumulated in the deep layer contributes to the formation of a lubricating water film layer with strong lubricity, thereby reducing the overall stability of loess slopes. Furthermore, the changed permeability stems from the conversion between micropores, small pores, mesopores, and macropores. Internal erosion forms a layer of clay particle aggregation at a certain depth, thereby promoting the formation of landslide slip surfaces. This study is highly significant as it contributes to in-depth elucidation of the mechanism underlying the impact of rainfall on the microstructure and unsaturated permeability characteristics of the loess.

Keywords: unsaturated seepage; internal erosion; microstructure evolution; migration of fine particle

1 Introduction

Loess, which is a typical aeolian fine-grained sediment that is widely distributed worldwide (Garakani et al., 2015), covers approximately 631,000 km^2 in China. Loess is mainly distributed in arid and semi-arid regions (Liu et al., 1964; Liu, 1985) and accounts for approximately 6.6% of the total land area of China. Loess formations within the Ili River Valley (hereafter referred to as the Ili loess) form a strip-like pattern and are mainly distributed in river terraces, low hills, and foothill slopes. The thickness of Ili loess generally ranges from several meters to nearly a hundred meters, and the deposition age is mostly after the last glacial period (Ye et al., 2003). The

https://doi.org/10.5194/egusphere-2026-1999
Preprint. Discussion started: 29 May 2026

increased frequency of extreme weather events globally and the enhanced intensity of human activities result in significant seasonal dynamic changes in terms of the moisture content or extreme geological events in the Ili River Valley. These changes lead to alterations in the matric suction of the soil mass, which affect the soil strength and trigger geological disasters such as loess landslides (Cui, 2014; Jianbing et al., 2014).

In summer, the Ili loess undergoes long-term infiltration of rainfall associated with the altered internal structure, thereby accelerating the occurrence of geological disasters (Wang et al., 2019). The Ili loess, which is characterized by large pores, water sensitivity, and loose texture, is prone to landslide disasters (Smalley, 2001). The loess with thick layers, owing to its vulnerability to internal erosion and dissolution, is referred to as "Karst soil" (Jianbing et al., 2014). Correspondingly, when fine particles—such as clay and silt—move through larger pores due to the action of seepage, the process is known as permeation (Bendahmane et al., 2008; Chapuis, 1992). Notably, when the internal structural characteristics of the soil are changed, internal erosion influences the stability of loess strata through a complex geological process. (Moffat et al., 2011; Peng et al., 2018). In contrast with surface erosion, internal erosion develops within the loess layer, where seepage mobilizes fine particles and redistributes them through the pore network (Bendahmane et al., 2008; Kenney and Lau, 1985; Zhuang et al., 2015a). Notably, the movement and loss of fine soil particles during the internal erosion process is expected to decrease the density and strength of loess (Mao, 2005; Richards and Reddy, 2007; Vallejo, 2001).

Considering the crucial role played by permeability, thoroughly elucidating the evolution of unsaturated permeability of the loess affected by rainfall is important. Previous studies have developed various methods and instruments to measure the unsaturated permeability (Gallage et al., 2013). However, owing to the low unsaturated permeability of loess and long duration of seepage tests, the current instrument is time-consuming (Ng and Leung, 2012). Compared with the steady-state method, the instantaneous profile method can shorten the duration of permeability testing. (Watson, 1966), as verified by Romero et al. (1999). Although the macroscopic characteristics of the loess are primarily determined by its microstructure structural features (Shao et al., 2018), rainfall causes changes in the original microstructure of loess and is not sufficient for explaining the evolution mechanism of unsaturated permeability of the loess (Wang et al., 2019). Therefore, the evolution of the loess microstructure induced by the rainfall infiltration should be investigated, and the corresponding microstructural characteristics of the loess should be determined.

Against the backdrop of the information above, three sets of rainfall infiltration tests with rainfall intensities of 10, 20, and 30 mm/h were carried out. The unsaturated permeability of Ili loess was then calculated based on the moisture content and matric suction monitored using sensors. Subsequently, scanning electron microscope tests and laser particle size analysis were conducted on the loess samples subjected to different rainfall intensities. Apart from the laboratory tests, the COMSOL Multiphysics was used to simulate the rainfall-induced seepage erosion process of the Ili loess. The discussion at the end of this paper highlights the evolution mechanism

https://doi.org/10.5194/egusphere-2026-1999
Preprint. Discussion started: 29 May 2026

of the microstructure and unsaturated permeability of loess affected by varying rainfall intensities. Additionally, the interaction mechanisms were explored.

2 Experimental Materials and Methods

2.1 Experimental Materials

The loess samples used in the present study were obtained from the Kalahaiyisu landslide in the eastern part of Xinyuan County, Ili region, China(Fig. 1). The landslide is a typical loess internal landslide with a slope direction of 320°, a longitudinal length of 500–580 m, a transverse width of 100–400 m, and an average slope gradient of 26. The slip surfaces of the landslide typically developed within the loess layer or at the interface between the loess layer and other strata (Kaidierding Wulamu et al., 2023). Fig. 1 shows that the geological strata are mainly composed of the loess, the erosion characteristics of which are primarily dominated by hydraulic and freeze-thaw erosion. Notably, the hydraulic erosion intensity near the loess sampling location reached extremely high levels owing to the long-term influence of rainfall and snowmelt infiltration. Table 1 presents the various physical characteristics of the loess samples, whereas Fig. 2 shows the particle size distribution of the loess samples. Evidently, the loess samples are classified as silty loess (Shepard, 1954) because they are predominantly composed of silt (approximately 79.1%). The sand and clay contents, at 10.08% and 10.82%, respectively, are considerably lower than the silt content. .

https://doi.org/10.5194/egusphere-2026-1999
Preprint. Discussion started: 29 May 2026

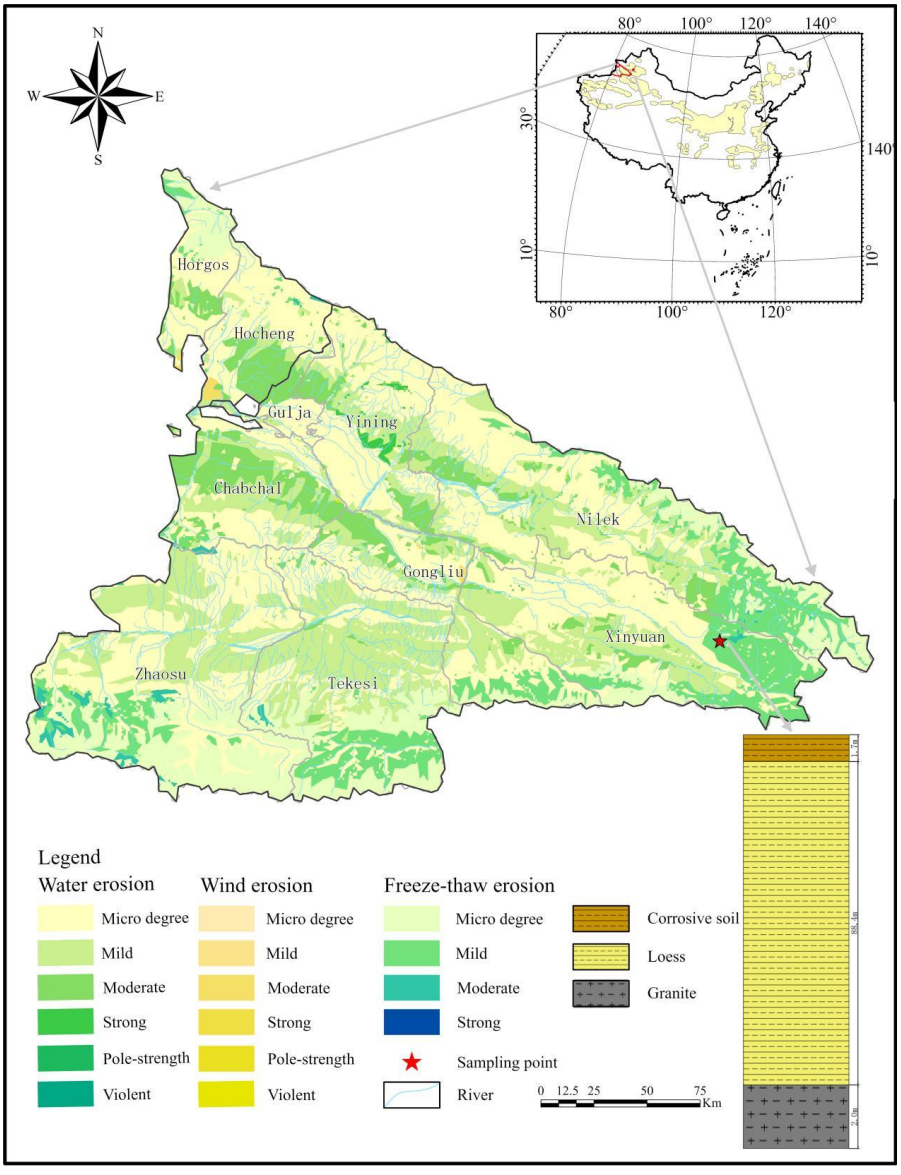

Fig. 1 Distribution of the sampling points and characteristics of their erosion (http://www.resdc.cn)

https://doi.org/10.5194/egusphere-2026-1999
Preprint. Discussion started: 29 May 2026

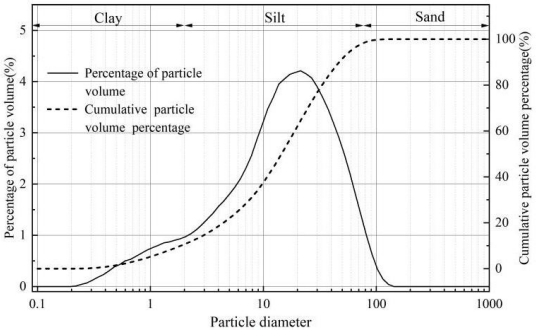

Fig. 2 Grain-size distribution curves of the tested loess

Table 1 Basic physical properties of the tested loess

Property	Value
Natural moisture content (%)	6.41
Porosity (%)	0.613
Liquid limit (%)	22
Plastic limit (%)	17
Natural density (g/cm^3)	1.43
Clay content (%)	10.82
Silt content (%)	79.1
Sand content (%)	10.08
Micropore area ratio (%)	2.15
Small pore area ratio (%)	5.68
Mesopore area ratio (%)	2.34

2.2 Permeation Test

2.2.1 Experimental Method

As shown in Fig. 3a, the self-designed cylindrical one-dimensional permeameter was developed to conduct unsaturated permeability tests. Both sides of the acrylic cylinder were uniformly perforated with 0.8 cm diameter holes, with vertical spacing of 10–20 cm. The distance between the first and second holes at the top was 10 cm, whereas the rest holes were spaced 20 cm apart. MTD-05 and MPS-6 sensors were installed through the side holes at different elevations along the soil column to record matric suction and volumetric water content during infiltration. The measurement range of the TEROS 21 matric potential sensor developed by the METER Group (Fig. 3c) ranges from −5 to 100,000 kPa, with an accuracy of 2 kPa. The resolution of the sensor is 0.1 kPa and the measurement frequency is 70 MHz. The MTD-05 humidity sensor (Fig. 3d) has a measurement range of 0%–100%, with a resolution of 0.1% and an accuracy of 3%. To allow water reaching the base of the soil column to drain smoothly, 5 mm drainage holes were uniformly arranged at the bottom of the cylindrical permeameter.. Notably, the rigid organic glass material was adopted to construct the permeameter because of budget limitations. However, a permeameter with flexible walls (Sadeghi and AliPanahi, 2020) should ideally be used because a

https://doi.org/10.5194/egusphere-2026-1999
Preprint. Discussion started: 29 May 2026

rigid permeameter does not reflect the volume changes that occur during soil saturation.

During the preparation of the soil columns, the loess powder collected onsite was air-dried, crushed, and sieved outdoors. Subsequently, tap water was uniformly sprayed onto the soil surface. Afterward, a mixer was adopted to achieve the natural moisture content (14.1%) for all samples before final sealing. All prepared samples were left to stand for 72 h to ensure uniform moisture distribution. The layered compaction method was adopted to prepare the loess columns and achieve a natural density of 1.65 g/cm³. The specific steps are presented below:

(1) The mass of soil required for a 10-cm-high soil column was calculated based on the dry soil density and natural moisture content, and batches of soil with the target moisture content were prepared in 10-cm increments.

(2) A layer of fast filter paper was placed at the bottom of the organic glass test barrel, after which the prepared moist soil was evenly spread in layers while sets of humidity sensors and matric potential sensors were buried at depths of 10, 20, 40, 60, and 80 cm.

(3) Steps (1) and (2) were repeated to prepare three sets of test soil columns.

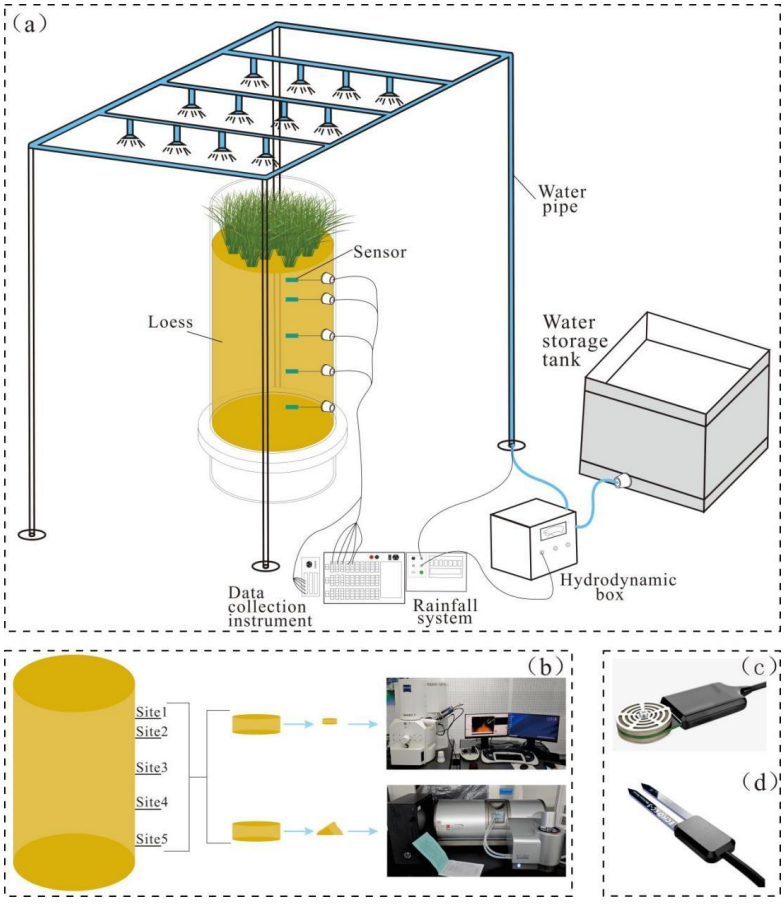

https://doi.org/10.5194/egusphere-2026-1999
Preprint. Discussion started: 29 May 2026

Fig. 3 Self-designed rainfall permeation test apparatus and microstructural testing equipment; (a) homemade rainfall test apparatus; (b) microstructural sample locations and sampling steps, along with microstructural testing equipment (SEM instrument and laser particle size analyzer); (c) and (d) matric suction and moisture content sensors

Moisture content variations in the Ili region are more pronounced at shallow depths (≤50 cm) under natural rainfall conditions. Therefore, sensors were embedded at different heights in the small holes of the soil column. To prevent erosion of the soil column surface, soil flaking, or water seepage along the sidewalls owing to rainfall and to better simulate the response of shallow loess in the study area to rainfall events, grass plants of the same variety as those in the study area were placed on the surface of the soil column. Rainfall was simulated using a watering system, and three rainfall intensities of 10, 20, and 30 mm/h were applied based on the rainfall characteristics of the study area, with a duration of 4 h for each intensity, resulting in three sets of experiments. Meanwhile, the sensors recorded real-time data on volumetric water content and matric suction.

2.2.2 Calculation of Unsaturated Permeability Coefficient

No surface ponding occurred during the infiltration experiment. Therefore, the advancement of the wetting front was treated as a one-dimensional vertical process for the calculation of the unsaturated permeability coefficient. The coefficient was determined by the instantaneous profile method using the measured changes in volumetric water content and matric suction during rainfall infiltration (Watson, 1966; Hamilton et al., 1981). The governing expression is given as follows:

$$\mathrm{h}_w=\mathrm{h}+\mathrm{h}_m \tag{1}$$

During infiltration, the total head h_w at any position in the soil column is equal to the sum of the position head h and the matric suction head h_m, as shown in Equation (1).

$$i_w=\frac{d\mathrm{h}_w}{d_z} \tag{2}$$

The hydraulic gradient i_w at any arbitrary time t is equal to the slope of the water head distribution line at that point, as shown in Equation (2).

$$V_w=\int_0^z \theta_w(\mathrm{h})_t A dz \tag{3}$$

In Equation (3), A represents the interface area of the soil column, and $\theta_w(\mathrm{h})_t$ is the volumetric water content. The seepage velocity v_w is calculated according to Equation (4).

$$v_w=\frac{dV_w}{Adt} \tag{4}$$

Permeability is expressed as follows:

$$k=\frac{v_w}{i_{ave}} \tag{5}$$

where i_{ave} is the average hydraulic gradient at point z at a certain moment, and is calculated as follows:

$$i_{ave}=\frac{1}{2}\left(\frac{\mathrm{h}_{w(z2),t1}-\mathrm{h}_{w(z1),t1}}{z_2-z_1}+\frac{\mathrm{h}_{w(z2),t2}-\mathrm{h}_{w(z1),t2}}{z_2-z_1}\right) \tag{6}$$

https://doi.org/10.5194/egusphere-2026-1999
Preprint. Discussion started: 29 May 2026

2.3 SEM Testing

SEM imaging combined with geometric visualization analysis was used to evaluate the pore characteristics and microstructure of remolded loess subjected to different rainfall intensities. The sampling and preparation procedures for the loess SEM test samples are shown in Figs. 3b and 4. First, after infiltration, samples were collected from depths of 10, 20, 40, 60, and 80 cm in the soil column using a ring cutter with a diameter of 61.8 mm and a height of 20 mm, which was pressed into the center of the soil column. The samples were then naturally dried to remove moisture. Precautions were taken to avoid disturbing the sample center during this process. The dried samples were subsequently ground and polished to produce SEM samples of suitable size for mounting on the specimen holder. Finally, the SEM samples were sputter-coated with gold and prepared for microstructural observation using a Sigma 300 field-emission SEM. To ensure accuracy in the microstructure observation and pore characterization, the central region of each microsample was selected for SEM observation.

Subsequently, the SEM images were processed via the Matlab software. SEM image processing generally constitutes three steps (Fig. 4): ① Contrast enhancement to clarify the boundaries between soil particles and pores; ② Noise reduction achieved through low-pass and median filtering for a more accurate and easier segmentation of SEM images; ③ Image segmentation was performed by assigning white to particles and black to pores, thereby enabling the separation of these two soil components (Li and Li, 2017; Liu et al., 2011). Pore structures in the SEM images were visualized based on Matlab software.

2.4 Laser Particle Size Analysis

The BT-9300S (SE) laser particle size analyzer was adopted to determine the particle size distribution using wet dispersion technology. The sampling and preparation procedures for the loess particle size distribution test samples are shown in Figs. 3b and 4. First, after infiltration, approximately 50 g of surface soil samples were collected from depths of 10, 20, 40, 60, and 80 cm in the soil column using a soil cutting knife. The samples were placed in aluminum boxes, oven-dried, and then transferred to sample containers for subsequent testing. During testing, the samples were initially crushed using a pestle, after which an appropriate amount of sample powder was added to the circulation tank of the laser particle size analyzer. Ultrasonic treatment was applied to disperse soil aggregates, after which the instrument automatically determined the particle-size distribution of the samples.

https://doi.org/10.5194/egusphere-2026-1999
Preprint. Discussion started: 29 May 2026

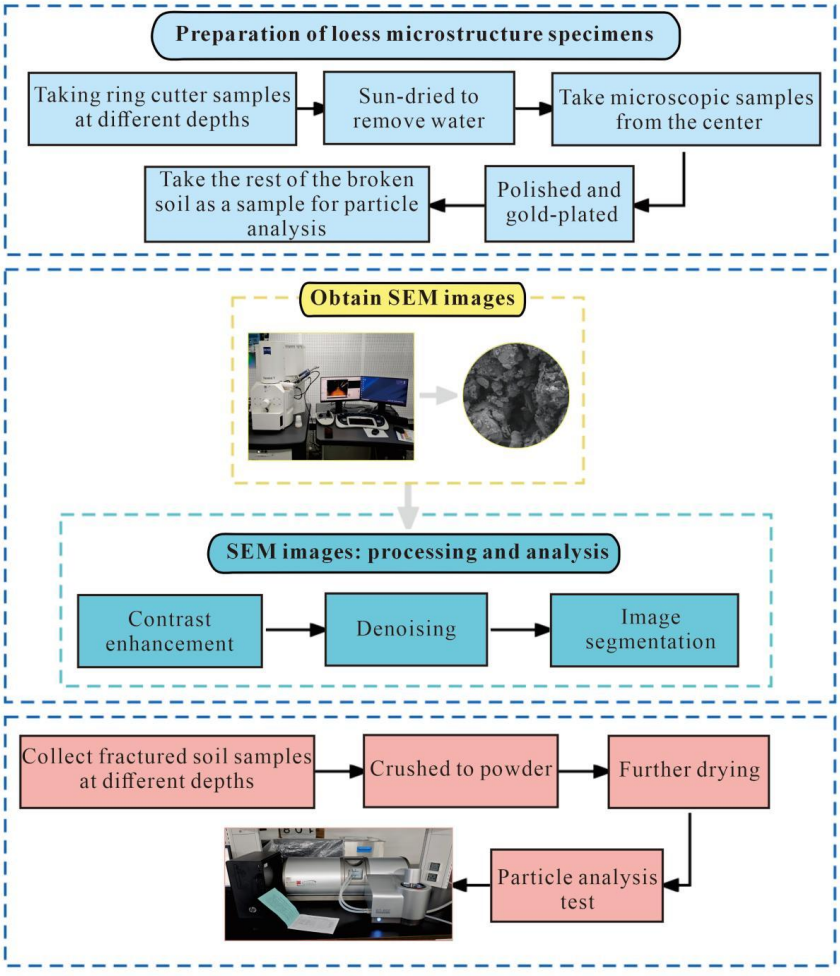

Fig. 4 Sample preparation for microstructural test and imaging process of SEM

2.5 Numerical Simulation in COMSOL Multiphysics

A numerical calculation model capable of accurately describing the seepage erosion process of soil under rainfall infiltration conditions was established based on the unsaturated seepage theory of porous media. The model was developed on the COMSOL Multiphysics numerical simulation platform using particle transport and erosion constitutive models. During construction of the numerical model, stable and unstable components were introduced, and the solid and liquid phases in saturated porous media were expanded into four-phase components to improve the description of mass transfer between fine particles in the solid and liquid phases (Schrefler, 2002).The migration of fine particles within the soil owing to hydraulic actions was considered by assuming that the porous medium consisted of four-phase components: stable solid-phase skeleton (ss), erodible solid-phase fine particles (se), liquid-phase

https://doi.org/10.5194/egusphere-2026-1999
Preprint. Discussion started: 29 May 2026

fine particles moving with the fluid flow (fe), and pure fluid (ff). The erosion constitutive model and the coupling relationship of the permeability coefficients were constructed in the software and used as cross-coupling terms in the multiphysics field. This enabled the numerical coupling of the particle transport control equations, porosity change control equations, and unsaturated seepage control equations, as illustrated in Fig. 5 (Duo et al., 2024).

The internal erosion process induced by seepage is primarily a two-way coupling process between seepage and fine particle migration. Therefore, when the coupling effect of seepage erosion was considered, the unsaturated soil satisfied both the unsaturated seepage control equations and the V–G model (van Genuchten, 1980). Notably, the actual density of liquefied fine particles should represent the difference between the fine particles detached from the soil solid phase and the deposited liquefied fine particles. However, owing to limitations in the measurement of deposited liquefied fine particles, the density of liquefied fine particles deposited within the soil skeleton could not be definitively determined. Therefore, this study did not consider the influence of this component and assumed that no deposition of liquefied particles occurred during particle migration (Duo et al., 2024). The basic loess parameters used in the numerical model calculations were partly obtained from experimental tests on Ili loess and partly adopted from previous studies (Hou and Fan, 2022), as presented in Table 2.

Table 2 Fundamental parameters and variables for numerical modelling

Parameters	Values/equation	Sources
Rainfall intensity	2.2E−6 [m/s]	
Critical seepage velocity	1.5E−16 [m/s]	Basic parameters of loess tested by authors
Initial saturated permeability coefficient	8.5E−6 [m/s]	
Fine particle density	1868 [kg/m^3]	
Erodible fine particle density	400 [kg/m^3]	Basic parameters of loess obtained from another research
Erodible particle density	$\rho_{se\infty}(v)=\begin{cases}\rho_{se0}-\left(\rho_{se0}-\rho^*_{se\infty}\right)v/v^* & (0\le v(t)\le v^*)\\ \rho^*_{se\infty}-\alpha_{er}lg(v/v^*) & \left(v^*\le v(t)\right)\end{cases}$	(Cividini et al., 2009)
Seepage erosion rate	$\rho^{ex,fe}(t,v)=\beta_{fe}\lvert v\rvert[\rho_{se}(t)-\rho_{se\infty}(v)]$	
Permeability coefficient variable	$k_0=\frac{n^3}{(1-n)^2}\times\frac{(1-n_0)^2}{n_0^3}k_{s0}$	(Xie et al., 1999)

https://doi.org/10.5194/egusphere-2026-1999
Preprint. Discussion started: 29 May 2026

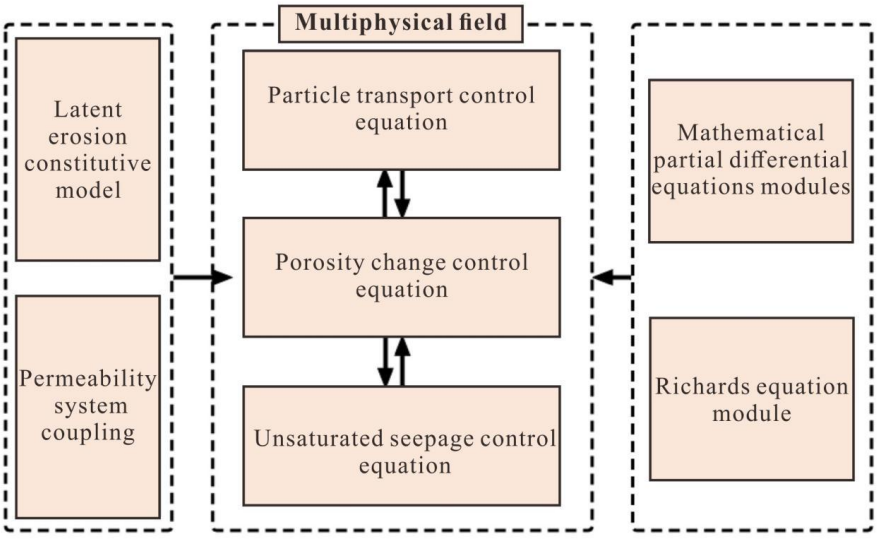

Fig. 5 Framework of the numerical model for computation

3 Experimental Results

3.1 Variation of Unsaturated Permeability Coefficient

The seepage depths of the three groups of soil columns were 64, 78, and 96 cm. Fig. 6 presents how the unsaturated permeability coefficient varies with volumetric water content under the three rainfall-intensity experiments. Fig. 6 shows that the unsaturated permeability coefficients of the three experimental groups were nearly identical when the volumetric water content was low. Therefore, the influence of rainfall intensity on the unsaturated permeability coefficient could be disregarded under low volumetric water content conditions. Noticeable differences among the unsaturated permeability coefficients of the three experimental groups were observed as the volumetric water content increased. For instance, at a volumetric water content of approximately 30%, the unsaturated permeability coefficients of the three experimental groups were 7.49E−4, 7.91E−4, and 9.97E−4. Fig. 6 also shows that the unsaturated permeability coefficients of the three experimental groups exhibited an exponential growth trend with increasing water content. Under a rainfall intensity of 30 mm/h, the unsaturated permeability coefficient exhibited higher values at elevated volumetric water contents, which, combined with the trends in the microstructural characteristics, suggests that internal erosion increased the internal porosity of the soil and consequently the maximum water content, while also affecting the rate of water transport within the soil under the same water content conditions.

https://doi.org/10.5194/egusphere-2026-1999
Preprint. Discussion started: 29 May 2026

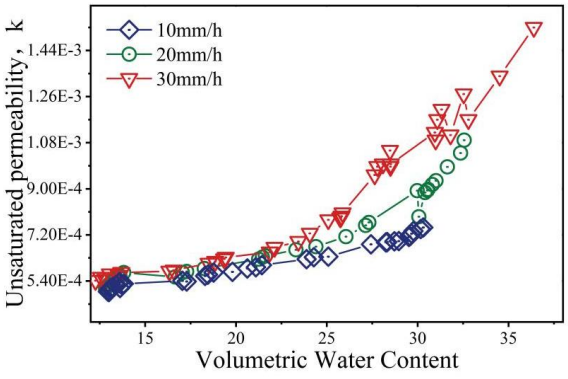

Fig. 6 Variation of unsaturated permeability coefficient after rainfall infiltration

3.2 Particle Migration Characteristics

Internal erosion in loess, which involves the migration of fine particles under water flow and the rearrangement of the soil particle skeleton, is one of the major causes of geological disasters in loess areas (Cui, 1992). After completion of the rainfall infiltration experiments under three different rainfall intensities, loose soil samples from five depths in each soil column were collected for particle analysis tests (Fig. 3b). Fig. 7 presents the cumulative particle-size distributions of the tested loess samples. Evidently, the particle size distributions at different depths in the experimental soil columns changed owing to rainfall-induced internal erosion, and the effect became more pronounced with increasing rainfall intensity. As shown in Fig. 7, with increasing sampling depth, the clay content in the samples increased significantly, whereas the sand content decreased notably. When the rainfall intensity was 10 mm/h, internal erosion primarily affected the clay content in layers 1 and 2 of the soil column, with clay contents higher than that in the original soil sample (Fig. 7a). At a rainfall intensity of 20 mm/h, the clay contents in layers 1 and 2 were lower than that in the original soil sample, with higher proportions of silt and sand than those in the original sample, whereas the clay contents in layers 3, 4, and 5 were higher than that in the original sample, with lower proportions of silt and sand than those in the original sample. Notably, the particle size distribution curve of layer 5 was very close to that of the original soil sample, indicating that although rainfall infiltration did not reach the depth of layer 5, migration of soil particles still affected the particle distribution in this region (Fig. 7b). At a rainfall intensity of 30 mm/h, the clay contents in layers 1–4 were lower than that in the original soil sample, with higher proportions of silt and sand, whereas the clay content in layer 5 was significantly higher than that in the original sample, with lower proportions of silt and sand (Fig. 7c). This result suggests that clay particles migrating from the upper layers of the soil column accumulated in the lower layers, leading to a significantly higher clay content than that in the original soil sample. The clay contents in each layer of the three groups of soil columns shown in Fig. 7d confirm this observation. Furthermore, comparison of the three experimental groups revealed that migration of fine clay particles within the loess became increasingly pronounced with increasing rainfall

https://doi.org/10.5194/egusphere-2026-1999
Preprint. Discussion started: 29 May 2026

intensity.

Larger particles commonly form the structural framework, whereas smaller particles fill the pores, with all particles bonded together (Cui et al., 2019). Previous studies have shown that fine particles in loess can migrate under intense rainfall conditions and accumulate at certain depths within the soil layer, thereby forming a lubricating water film that may promote geological disasters in loess formations (Lu et al., 2010; Zhuang et al., 2015b).

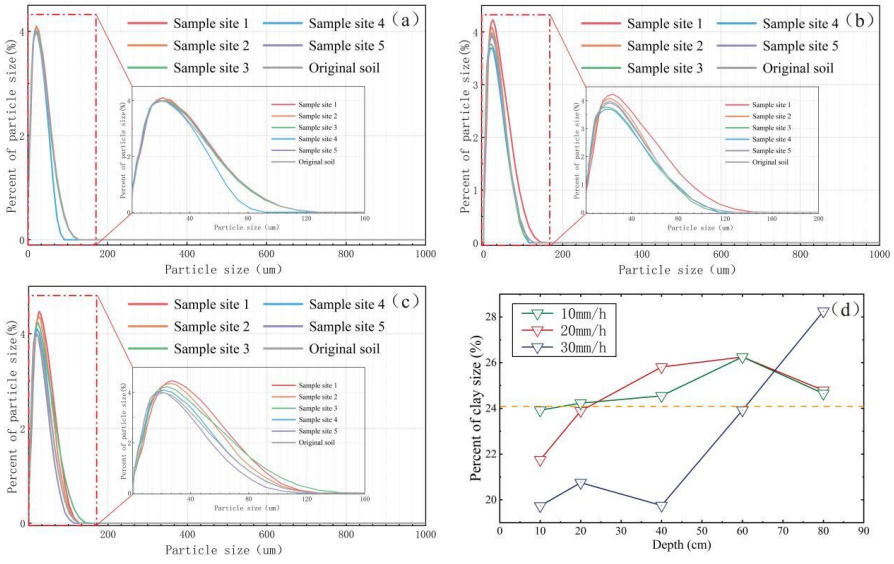

Fig. 7 Particle size distribution at different locations in the soil columns after rainfall infiltration: (a)–(c) particle size distribution curves; (d) clay content in each layer of the soil columns

3.3 Evolution of Pore Characteristics

Loss of particles in loess is typically caused by dissolution, degradation, erosion, and migration, among other factors. Regardless of the cause, soil particle loss results in destruction of the soil composition and microstructure (Skempton and Brogan, 1994). Variations in the areas of different pore types in the SEM test samples are shown in Fig. 8.

microstructural images of the soil columns at different depths were obtained through SEM testing, and the pore area ratios of the soil samples were derived from the SEM images. Fig. 8 illustrates the variations in the areas of different pore types at different sampling depths in the three groups of experimental soil columns after erosion under different rainfall intensities. Overall, the total pore area increased with increasing rainfall intensity, and under a rainfall intensity of 30 mm/h, macropores appeared in the samples from the top of the soil column. As the sampling depth increased, the area proportions of micropores and small pores increased, whereas those of macropores and mesopores decreased. Before infiltration, the predominant pores in the loess were medium and small pores, with strong pore connectivity, resulting in a relatively high initial permeability coefficient. After infiltration, the pore

https://doi.org/10.5194/egusphere-2026-1999
Preprint. Discussion started: 29 May 2026

distributions at different depths of the soil column changed differently, with decreases in total pore area and increases in the proportion of micropore area at greater depths. Closer to the surface of the soil column, the total pore area increased, with larger pores and mesopores accounting for greater proportions. The variations in the areas of different pore types with infiltration depth confirm the migration of fine soil particles and explain the decrease in the unsaturated permeability coefficient with infiltration.

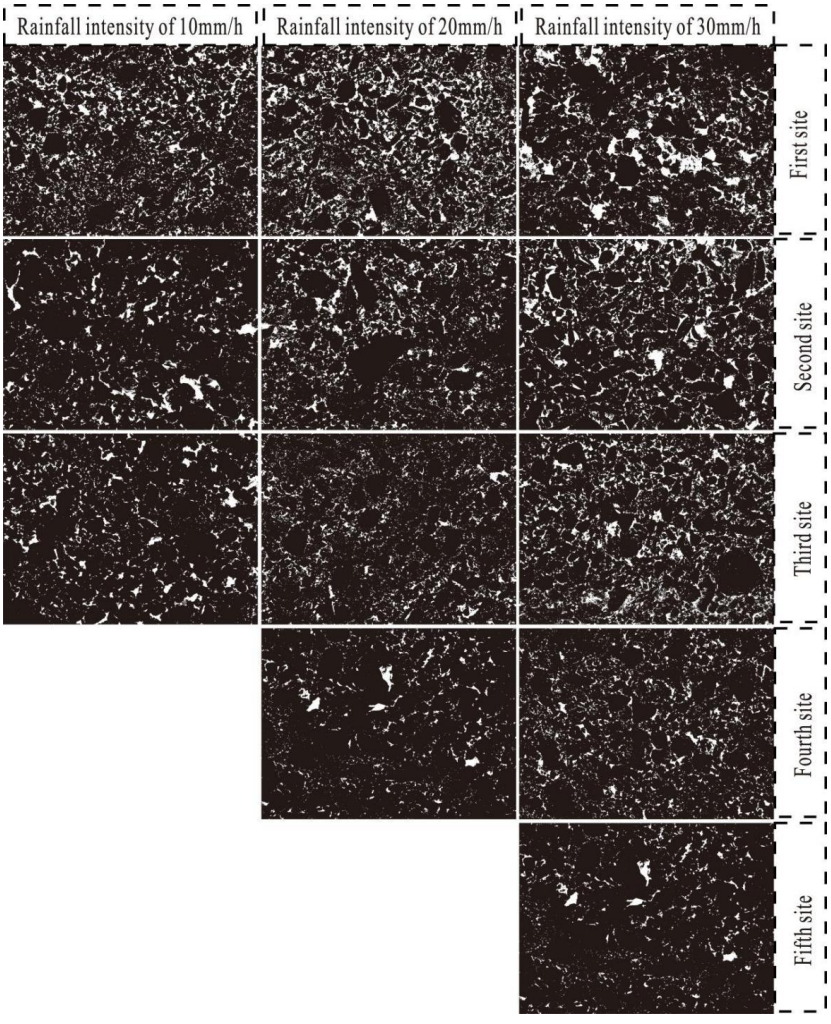

Fig. 8 Pore distribution at different locations in three soil columns after rainfall infiltration

Fig. 9 presents the percentages of various pore area types relative to the SEM image area at different sampling depths in the three soil columns after erosion under different rainfall intensities. Evidently, the total pore area ratio increased with increasing rainfall intensity and decreased with increasing infiltration depth. At a rainfall intensity of 10 mm/h, the total pore area ratio increased by 2.93% at the top

https://doi.org/10.5194/egusphere-2026-1999
Preprint. Discussion started: 29 May 2026

sampling point and decreased by 2.47% at the maximum infiltration depth. Under a rainfall intensity of 20 mm/h, the total pore area ratio increased by 3.57% at the top sampling point and decreased by 2.56% at the maximum infiltration depth. At a rainfall intensity of 30 mm/h, macropores appeared at the top sampling point of the soil column, with a relatively high area ratio of 1.24%, and the total pore area ratio increased significantly by 8.4%. The pore area ratio at the maximum infiltration depth also decreased significantly by 5.46%. Thus, the changes in permeability can be inferred to result from the conversion among micropores, small pores, mesopores, and macropores. Additionally, the proportion of micropores within the total pore area showed no significant change, indicating that infiltration had only a minor impact on micropores in the loess. Fig. 10 shows that rainfall had varying impacts on the porosity at different depths of the loess soil columns. After infiltration, the porosity of the shallow surface layer of the soil column significantly exceeded the initial porosity, and this effect became more pronounced with increasing rainfall intensity and infiltration depth. This finding confirms the evolution pattern of pore size in loess induced by infiltration, as observed in Figs. 8 and 9.

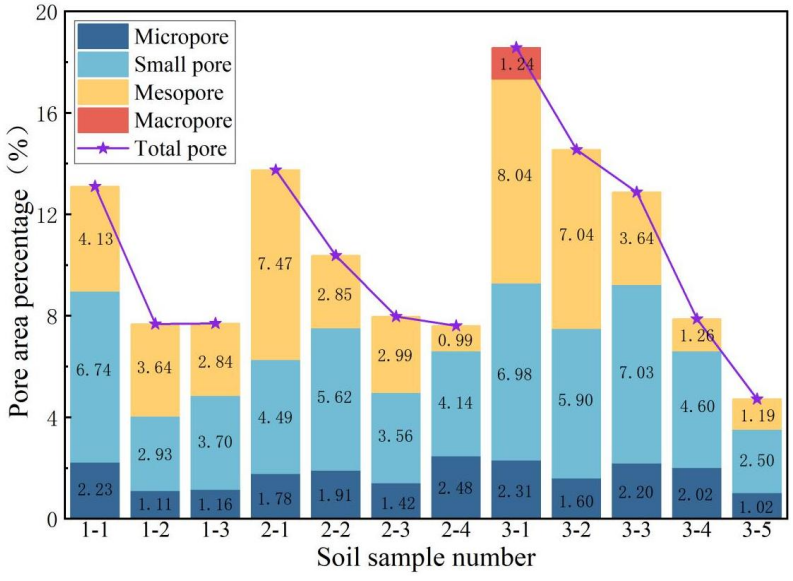

Fig. 9 Pore-area percentages measured at different heights in the three soil columns after rainfall infiltration

https://doi.org/10.5194/egusphere-2026-1999
Preprint. Discussion started: 29 May 2026

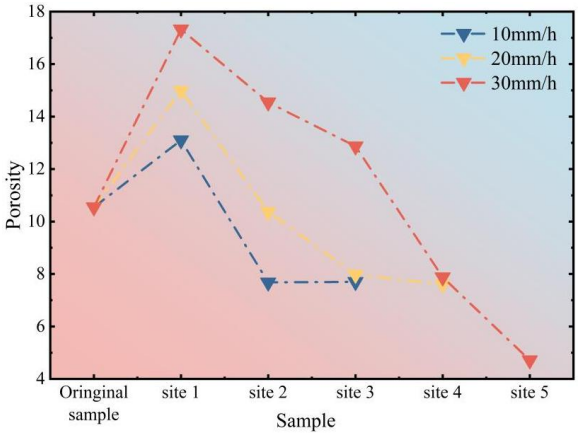

Fig. 10 Porosity measured at different heights in the three soil columns after rainfall infiltration

3.4 microstructural Structural Morphology

Fig. 11 presents SEM images of the in-situ loess, as well as the shallow surface layer and deeper layers after infiltration, showing varying degrees of change in the microstructural structure of the loess at different depths after infiltration. Fig. 11a illustrates the microstructural features of the loess before infiltration, characterized by coexistence of different pore sizes, numerous clay particles adhering mainly to the surfaces of larger particles, and a relatively compact structure. Fig. 11b shows that after rainfall, the microstructural structure of the soil sample from the shallow surface layer of the soil column evolved from an embedded structure into a looser framework structure with large pores and microaggregates. Detachment and migration of connecting and clay particles adhering to the surfaces of larger particles led to transformation of more micropores and small pores into mesopores or macropores. Fig. 11c shows that after rainfall infiltration, the microstructural structure at deeper depths of the experimental loess column exhibited a micropore-cemented structure, with a denser arrangement dominated by micropores and small pores.

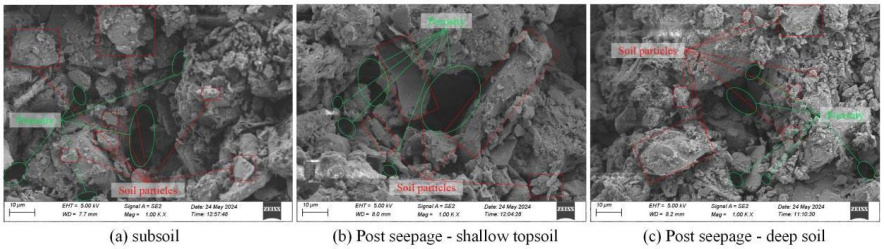

(a) subsoil (b) Post seepage - shallow topsoil (c) Post seepage - deep soil

Fig. 11 microstructural structure of loess samples before and after rainfall infiltration

The amounts of fine clay particles and clay particles adhering to the particle skeleton and filling the pores between the skeleton are significantly greater than those in the original in-situ soil sample. Consequently, under infiltration conditions, loss of fine clay particles results in clearer particle contours and skeleton structures in the

https://doi.org/10.5194/egusphere-2026-1999
Preprint. Discussion started: 29 May 2026

shallow surface layer of the loess. The migrated fine clay particles accumulate in the deeper soil layers, leading to higher contents of fine clay and adhering particles, thereby confirming the aforementioned particle migration process. Generally, contact between large particles forms a framework structure, creating a soil skeleton that is looser than that of an embedded structure, with larger pore areas and hence lower stability. In contrast, a cemented structure features a denser arrangement of particles, with pores filled by fine or clay particles, resulting in greater stability than those of framework and embedded structures.

3.5 Numerical Calculation Results

The cloud maps of erodible particle content distribution in the soil column model at different stages are presented in Fig. 12; these results were obtained from the numerical simulations. Generally, loss of fine particles in soil is related to the infiltration velocity; therefore, the concentration of erodible fine particles is linked to the rate at which the wetting front advances downward in unsaturated soil. The variation in erodible fine particle concentration shown in Fig. 12 is consistent with the infiltration process, and loss of fine particles occurs only within the infiltration-erosion zone. As rainfall duration increases, loss of erodible fine particles becomes more pronounced. This result is consistent with the particle migration patterns observed in the one-dimensional soil column infiltration experiments. Figs. 13a–c show the variations in erodible fine particle concentration, permeability coefficient, and soil porosity at different time intervals in the X = 0.15 m section of the numerically simulated soil column. Fig. 13 shows that during infiltration, the concentration of erodible particles, permeability coefficient, and soil porosity exhibited consistent variation patterns with soil depth and infiltration duration.

The numerical simulation results indicate that soil porosity continuously increased with ongoing rainfall infiltration, resulting in enhanced permeability. Furthermore, as the erosion process continued, the soil infiltration rate increased, allowing more water to infiltrate the deeper soil layers within the same time frame. These results suggest that loss of fine particles from the soil increased soil porosity, thereby enhancing permeability. The increase in permeability could further intensify the erosion process within the soil. Overall, good agreement was obtained between the numerical simulation results and the patterns observed in the one-dimensional soil-column rainfall infiltration experiments.

https://doi.org/10.5194/egusphere-2026-1999
Preprint. Discussion started: 29 May 2026

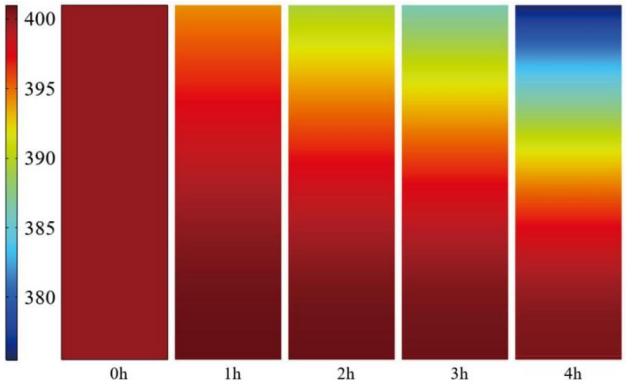

Fig. 12 Cloud maps of erodible particle content distribution at different stages in the numerical model

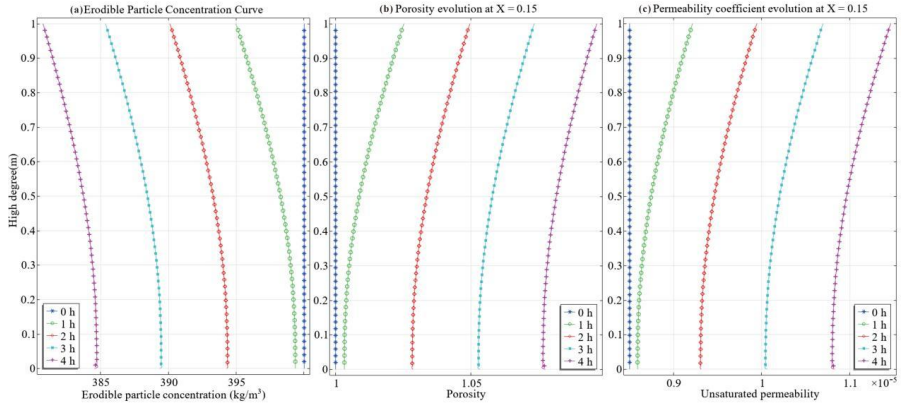

Fig. 13 Variation curves of critical parameters at different stages in the model section at X = 0.15 m: (a) erodible fine particle concentration; (b) soil porosity; and (c) permeability coefficient

4 Discussion

In the present study, rainfall experiments and microstructural observations were combined with numerical simulations results to examine the rainfall-induced evolution of the unsaturated permeability coefficient of loess and the associated influence of seepage on its microstructural characteristics. This section further discusses how rainfall-induced seepage modifies the microstructure of loess, how its unsaturated permeability coefficient evolves during infiltration, and how these changes affect the stability of loess landslides.

4.1 Microstructural Response of Loess to Rainfall Infiltration

The external factors causing loess collapsibility are mainly attributed to weakening of the interparticle bonding in loess owing to loss of calcium cementing materials and clay particles during rainfall infiltration (Bakhshipour et al., 2016; Meng and Li, 2019). As reported by Jiang et al. (2014), rainfall infiltration increases

https://doi.org/10.5194/egusphere-2026-1999
Preprint. Discussion started: 29 May 2026

the self-weight of the soil, this process weakens the bonding between soil particles and destabilizes the macropore framework, allowing particle rearrangement and ultimately enhancing the collapsible behavior of loess..

Figs. 11a and 14 illustrate the microstructure of the experimental loess before infiltration, characterized by high proportions of small pores and mesopores and coexistence of point and face contacts between soil particles. These features provide effective pathways for water infiltration and soil particle migration. Similar findings were reported by An et al. (2013) and Zhang (2019), who noted that under infiltration conditions, soil particles migrate downward, thereby altering the original particle arrangement and microstructural characteristics of loess. This finding is consistent with studies on Malan loess from the Loess Plateau, which revealed that fine particles are displaced under seepage, leading to a reorganization of the original particle framework.

Particle analysis revealed that under rainfall conditions, the clay particle content in the upper layer of the soil column decreased significantly, whereas that in the lower layer exceeded that in the original soil sample. These results suggest that during infiltration, soil aggregates dispersed and clay particles migrated downward under the influence of infiltration, accumulated in the lower layers, and filled the original pores, thereby forming additional soil aggregates. Correspondingly, SEM test results confirmed this conclusion: after rainfall erosion, the proportion of total pore area in the upper layer of the soil column increased significantly, whereas the proportion of micropore area decreased, resulting in a looser microstructure. Conversely, the deeper soil layers exhibited the opposite trend, with smaller pore area ratios than those in the initial soil sample and structures dominated by micropores and denser arrangements. The study reveals that rainfall erosion can cause vertical redistribution of the microstructural characteristics of Ili loess, including rearrangement of soil particles and pore characteristics, as well as restructuring of the microstructure. Overall, after rainfall erosion, the microstructural structural characteristics of Ili loess exhibited a loose structure with higher porosity in the upper layers and a dense structure dominated by small pores in the lower layers.

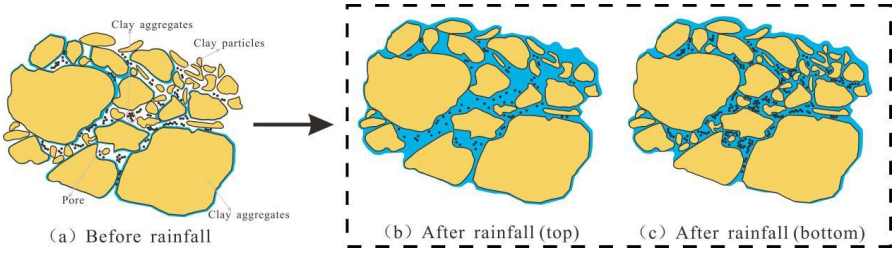

Fig. 14 Schematic representation of rainfall-induced changes in the loess microstructure

4.2 Mechanism Underlying Changes in the Unsaturated Permeability Coefficient

As demonstrated by Daigle and Dugan (2011), soil permeability is largely governed by the architecture of the pore network, connectivity, and pore arrangement.

https://doi.org/10.5194/egusphere-2026-1999
Preprint. Discussion started: 29 May 2026

Existing studies have primarily focused on the initial pore structure formed during soil sample preparation and have used it as the basis for studying and evaluating the seepage behavior of loess (Delage et al., 1996; Romero, 2013). However, this initial microstructure represents only part of the characteristics of loess, whereas the actual microstructure continuously changes during seepage. Therefore, investigating the effects of seepage on reshaping the microstructure and permeability of loess is essential.

The rainfall experiments indicate that the unsaturated permeability coefficient of Ili loess increases with increasing soil moisture content. As discussed earlier, during seepage, clay particles migrate downward with water flow, thereby altering the originally uniform distribution of soil particles and forming a loose structure in the upper layer and a dense structure in the lower layer. This process also results in a higher pore area proportion in the upper layer and a lower proportion in the deeper layers of the loess, as shown in Fig. 15. Consequently, seepage pathways in the deeper soil layers are obstructed by the migrated clay particles, leading to a decrease in the pore area ratio and, consequently, a decrease in the unsaturated permeability coefficient of the loess. Additionally, calcium cementing materials in the loess continuously disintegrate during seepage, thereby reducing the bonding between loess particles, which may increase the unsaturated permeability coefficient of the loess (Gratchev and Towhata, 2011).

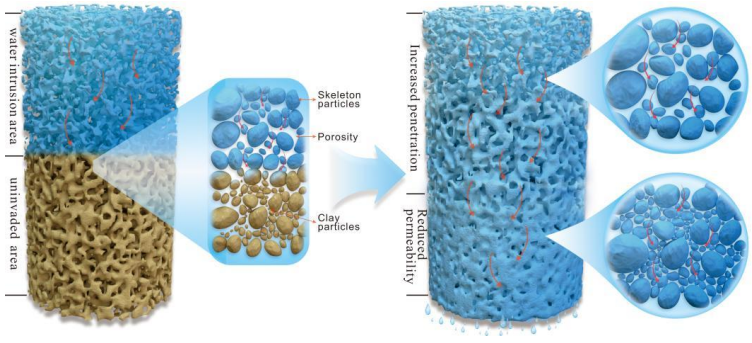

Fig. 15 Schematic representation of rainfall-induced changes in the internal structure and unsaturated permeability coefficient of loess

Mesopores and macropores play an important role in promoting interconnection between pores and increasing the water surface area. Evidently, as shown in Fig. 15, migration of clay particles leads to blockage of more mesopores and macropores, transforming them into small pores and micropores. The connectivity of small pores and micropores is lower than that of mesopores and macropores, and the saturated water surface area in small pores and micropores is smaller than that in mesopores and macropores. Consequently, the density in the deeper soil layers is higher, and the unsaturated permeability coefficient decreases with increasing soil density. Dafalla et al. (2020) found that during seepage, water first fills micropores under higher suction conditions. As shown in Fig. 9, the sensitivity of micropores to rainfall erosion can be disregarded, whereas the deeper pores in the loess are dominated by micropores after seepage. Therefore, after rainfall, the unsaturated permeability coefficient in the

https://doi.org/10.5194/egusphere-2026-1999
Preprint. Discussion started: 29 May 2026

deeper layers of the loess is smaller, and the increasing trend with increasing moisture content can be disregarded.

4.3 Engineering Significance

Water is one of the key factors contributing to geological hazards in loess areas. Particularly during prolonged heavy rainfall or extreme weather events such as storms, rainwater infiltration can potentially trigger significant geological disasters (Wu et al., 2021). Permeability is an important characteristic describing the internal pore flow capacity of loess and is crucial for evaluating its hydrogeological and engineering-geological properties (Cheng et al., 2021; Lee and Ho, 2009). Taking the Karahayisul loess landslide in Xinyuan County, Xinjiang, as an example, Kai et al. (2023) found that rainfall and snowmelt infiltration play major controlling roles in the stability of this loess landslide. Therefore, investigating rainfall-induced changes in the microstructural characteristics and structural stability of Ili loess is of great significance for evaluating the stability of loess landslides in the Ili region..

Fig. 16 illustrates the mechanism by which rainfall-induced changes in loess microcharacteristics affect the stability of loess slopes. Under rainfall conditions, migration of fine soil particles through the macropores in the soil leads to collapse and failure of the upper soil layers. Particle aggregation occurs in the deeper soil layers, thereby blocking effective water seepage pathways and transforming macropores into small pores. Experimental results indicate that greater rainfall intensity results in stronger seepage-induced internal erosion. In loess slopes, seepage-induced internal erosion can create a layer of clay particle aggregation at a certain depth within the loess, thereby further promoting formation of landslide slip surfaces and providing the necessary conditions for loess slope failure.

The increase in moisture content produces an exponential rise in the unsaturated permeability coefficient of loess.. At low moisture contents, the influence of rainfall intensity on the unsaturated permeability coefficient can be neglected, whereas at higher moisture contents, greater rainfall intensity results in a higher unsaturated permeability coefficient. Under these conditions, internal erosion in the loess becomes stronger with increasing permeability, thereby weakening the stability of loess slopes and increasing the likelihood of landslides. Therefore, clarifying how rainfall affects the evolution of loess microstructure and the unsaturated permeability coefficient can improve our understanding of loess landslide deformation and support early warning and prevention efforts in loess-prone areas..

https://doi.org/10.5194/egusphere-2026-1999
Preprint. Discussion started: 29 May 2026

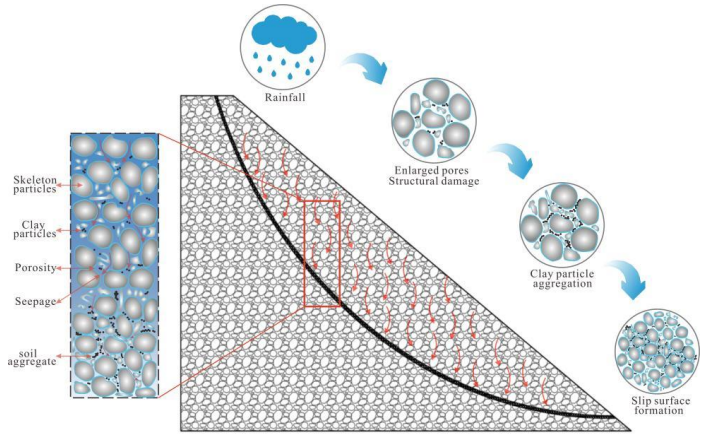

Fig. 16 Schematic diagram of how rainfall-induced microstructural evolution influences loess slope stability

5. Conclusions

TThree rainfall experiments with different intensities were performed using a self-designed one-dimensional rainfall infiltration device to examine the internal erosion process of Ili loess and the mechanism controlling changes in its unsaturated permeability coefficient. Samples collected after rainfall were subjected to SEM testing and laser particle size analysis. Additionally, COMSOL Multiphysics was used to simulate the seepage erosion process of loess under rainfall conditions. The experimental observations and numerical simulation results were used to examine changes in loess microcharacteristics before and after rainfall and to discuss the rainfall-induced evolution of the unsaturated permeability coefficient.. The engineering significance reflected by the evolution of loess microstructure and unsaturated permeability coefficient was also explored. The principal findings of this study are summarized as follows:

(1) The unsaturated permeability coefficient of loess exhibited an exponential increase with increasing moisture content. The changes in permeability resulted from conversion among small pores, micropores, mesopores, and macropores. Under seepage conditions, the pore distributions at different depths in the loess underwent different changes. The deeper regions exhibited decreases in total pore area and increases in the proportion of micropore area, whereas regions closer to the soil column surface exhibited increases in total pore area and higher proportions of macropores and mesopores.

(2) Migration of clay particles modified the soil microstructure, leading to increased porosity and permeability. This process resulted in substantial depletion of clay particles in the shallow loess layers, whereas these particles accumulated in deeper regions. In these deeper regions, the accumulated clay particles contributed to formation of a lubricating water film with strong lubricity, consequently decreasing the overall stability of the loess.

(3) Rainfall seepage exacerbated internal damage in the loess, causing pore reconfiguration and increased permeability. As internal erosion progressed, clay

https://doi.org/10.5194/egusphere-2026-1999
Preprint. Discussion started: 29 May 2026

particles accumulated at a certain depth, forming a concentrated layer. This layer facilitated development of a potential sliding surface, thereby creating conditions conducive to loess slope failure and landslides.

(4) The unsaturated permeability coefficient is one of the crucial physical properties of loess and can significantly influence its engineering properties (Bagarello et al., 2009). Loess in China is widely distributed, mainly in the Loess Plateau and the Ili River Valley. Based on particle composition, loess can be classified as cohesive, silty, or sandy (Gao et al., 2021). In this study, silty loess from the Ili River Valley was examined, with emphasis on the impacts of rainfall erosion and subsequent microstructural changes on the unsaturated permeability coefficient. The objective was to elucidate the evolution of the permeability coefficient under rainfall conditions and its relationship with loess microstructure. Although the findings may provide insights applicable to other regions containing similar silty loess, their generalizability remains limited because evidence regarding sandy and cohesive loess is still insufficient.

Data Availability

Data supporting the analyses presented in this paper are available from the corresponding author upon reasonable request.

Author Contributions

A.T., K.W., and Z.Z. framed the study plan and wrote the paper; Z.Z. provided research funding; A.T., K.W., Z.Z., R.L., and Y.Z. conducted relevant field research and visits; A.T., K.W., and R.L. conducted article data processing; Q.L., R.L., Y.Z., and X.Z. provided feedback on the manuscript. All authors have read and agreed to the published version of the manuscript.

Competing Interests

The authors declare that they have no conflict of interest.

Acknowledgements

The authors gratefully acknowledge support from the National Natural Science Foundation of China (42367021) and the Xinjiang Uygur Autonomous Region “Tianshan Yingcai” Scientific Research Program (2023TSYCCX0010).

Financial Support

This study was supported by the National Natural Science Foundation of China (42367021) and the Xinjiang Uygur Autonomous Region “Tianshan Yingcai” Talent Cultivation Program (2023TSYCCX0010).

https://doi.org/10.5194/egusphere-2026-1999
Preprint. Discussion started: 29 May 2026

References

An, P., Zhang, A. J., Liu, H. T., and Wang, T.: Degradation mechanism of long-term seepage and permeability analysis of remolded saturated loess, Rock Soil Mech., 34, 1965–1971, 2013 (in Chinese).

Bagarello, V., Sferlazza, S., and Sgroi, A.: Testing laboratory methods to determine the anisotropy of saturated hydraulic conductivity in a sandy-loam soil, Geoderma, 154, 52–58, 2009.

Bakhshipour, Z., Asadi, A., Huat, B. B. K., Sridharan, A., and Kawasaki, S.: Effect of acid rain on geotechnical properties of residual soils, Soils Found., 56, 1008–1020, https://doi.org/10.1016/j.sandf.2016.11.006, 2016.

Bendahmane, F., Marot, D., and Alexis, A.: Experimental parametric study of suffusion and backward erosion, J. Geotech. Geoenviron. Eng., 134, 57–67, 2008.

Cheng, Q., Tang, C. S., Xu, D., Zeng, H., and Shi, B.: Water infiltration in a cracked soil considering effect of drying-wetting cycles, J. Hydrol., 593, 125640, 2021.

Chapuis, R. P.: Similarity of internal stability criteria for granular soils, Can. Geotech. J., 29, 711–713, 1992.

Cividini, A., Bonomi, S., Vignati, G. C., and Gioda, G.: Seepage-induced erosion in granular soil and consequent settlements, Int. J. Geomech., 9, 187–194, 2009.

Cui, P.: Study on conditions and mechanisms of debris flow initiation by means of experiment, Chin. Sci. Bull., 37, 759–759, 1992.

Cui, P.: Progress and prospects in research on mountain hazards in China, Prog. Geogr., 33, 145–152, https://doi.org/10.11820/dlkxjz.2014.02.001, 2014 (in Chinese).

Cui, Y., Jiang, Y., and Guo, C.: Investigation of the initiation of shallow failure in widely graded loose soil slopes considering interstitial flow and surface runoff, Landslides, 16, 815–828, 2019.

Dafalla, M. A., Al-Mahbashi, A. M., Almajed, A., and Al-Shamrani, M.: Predicting soil-water characteristic curves of clayey sand soils using area computation, Math. Probl. Eng., 2020, 4548912, https://doi.org/10.1155/2020/4548912, 2020.

Daigle, H. and Dugan, B.: An improved technique for computing permeability from NMR measurements in mudstones, J. Geophys. Res. Solid Earth, 116, https://doi.org/10.1029/2011JB008353, 2011.

Delage, P., Audiguier, M., Cui, Y.-J., and Howat, M. D.: Microstructure of a compacted silt, Can. Geotech. J., 33, 150–158, 1996.

Duo, H., Xie, S., Jian, W., Wang, H., and Guo, C.: Characterization of dominant flow potential erosion at soil-rock interface of spherically weathered granite-like soil slopes, Geotechnics, 45, 950–960, https://doi.org/10.16285/j.rsm.2023.0644, 2024.

Gallage, C., Kodikara, J., and Uchimura, T.: Laboratory measurement of hydraulic conductivity functions of two unsaturated sandy soils during drying and wetting processes, Soils Found., 53, 417–430, https://doi.org/10.1016/j.sandf.2013.04.004, 2013.

Gao, C., Xu, L., Coop, M. R., Huang, C., and Zuo, L.: An investigation of particle breakage in loess, Eng. Geol., 286, 106083, 2021.

Garakani, A. A., Haeri, S. M., Khosravi, A., and Habibagahi, G.: Hydro-mechanical behavior of undisturbed collapsible loessial soils under different stress state conditions, Eng. Geol., 195, 28–41, https://doi.org/10.1016/j.enggeo.2015.05.026, 2015.

Gratchev, I. and Towhata, I.: Compressibility of natural soils subjected to long-term acidic contamination, Environ. Earth Sci., 64, 193–200, 2011.

https://doi.org/10.5194/egusphere-2026-1999
Preprint. Discussion started: 29 May 2026

Hamilton, J. M., Daniel, D. E., and Olson, R. E.: Measurement of hydraulic conductivity of partially saturated soils, Am. Soc. Test. Mater., Spec. Tech. Publ., 182–196, 1981.

Hou, X. and Fan, H.: Characterization of rainfall infiltration in unsaturated fissured soil based on COMSOL Multiphysics, Geotechnics, 43, 563–572, https://doi.org/10.16285/j.rsm.2021.0854, 2022.

Jiang, M., Zhang, F., Hu, H., Cui, Y., and Peng, J.: Structural characterization of natural loess and remolded loess under triaxial tests, Eng. Geol., 181, 249–260, https://doi.org/10.1016/j.enggeo.2014.07.021, 2014.

Jianbing, P., Hungchou, L. I. N., Qiyao, W. A. N. G., Jianqi, Z., Yuxiang, C., and Xinghua, Z.: The critical issues and creative concepts in mitigation research of loess geological hazards, J. Eng. Geol., 22, 684–691, https://doi.org/10.13544/j.cnki.jeg.2014.04.014, 2014.

Kaidierding Wulamu, Zhang, Z., Zhang, Y., Zhu, J., and Chen, W.: COMSOL Multiphysics-based calculation model of critical rainfall threshold for rainfall-induced landslide: A case study of Karahayisu landslide in Xinyuan County, Xinjiang, J. Eng. Geol., 31, https://doi.org/10.13544/j.cnki.jeg.2023-0206, 2023.

Kenney, T. C. and Lau, D.: Internal stability of granular filters, Can. Geotech. J., 22, 215–225, 1985.

Lee, K. T. and Ho, J. Y.: Prediction of landslide occurrence based on slope-instability analysis and hydrological model simulation, J. Hydrol., 375, 489–497, 2009.

Li, X. A. and Li, L. C.: Quantification of the pore structures of Malan loess and the effects on loess permeability and environmental significance, Shaanxi Province, China: An experimental study, Environ. Earth Sci., 76, 523, 2017.

Liu, C., Shi, B., Zhou, J., and Tang, C.: Quantification and characterization of microporosity by image processing, geometric measurement and statistical methods: Application on SEM images of clay materials, Appl. Clay Sci., 54, 97–106, 2011.

Liu, T. S.: Loess and the environment, China Ocean Press, Beijing, 237 pp., 1985 (in Chinese).

Liu, T. S., Wang, T. M., Wang, K. L., and Wen, C. C.: Loess on the middle reaches of the Yellow River, Science Press, Beijing, 234 pp., 1964 (in Chinese).

Lu, X., Cui, P., Hu, K., and Zhang, X.: Initiation and development of water film by seepage, J. Mt. Sci., 7, 361–366, 2010.

Mao, C. X.: Study on piping and filters: Part 1 of piping, Rock Soil Mech., 26, 209–215, 2005.

Meng, J. and Li, X.-A.: Effects of carbonate on the structure and properties of loess and the corresponding mechanism: An experimental study of the Malan loess, Xi'an area, China, Bull. Eng. Geol. Environ., 78, 4965–4976, https://doi.org/10.1007/s10064-018-01457-z, 2019.

Moffat, R., Fannin, R. J., and Garner, S. J.: Spatial and temporal progression of internal erosion in cohesionless soil, Can. Geotech. J., 48, 399–412, 2011.

Ng, C. W. W. and Leung, A. K.: Measurements of drying and wetting permeability functions using a new stress-controllable soil column, J. Geotech. Geoenviron. Eng., 138, 58–68, https://doi.org/10.1061/(ASCE)GT.1943-5606.0000560, 2012.

Peng, J. B., Sun, P., Igwe, O., and Li, X.: Loess caves, a special kind of geo-hazard on Loess Plateau, northwestern China, Eng. Geol., 236, 79–88, 2018.

Richards, K. S. and Reddy, K. R.: Critical appraisal of piping phenomena in earth dams, Bull. Eng. Geol. Environ., 66, 381–402, 2007.

Romero, E.: A microstructural insight into compacted clayey soils and their hydraulic properties, Eng. Geol., 165, 3–19, 2013.

https://doi.org/10.5194/egusphere-2026-1999
Preprint. Discussion started: 29 May 2026

Romero, E., Gens, A., and Lloret, A.: Water permeability, water retention and microstructure of unsaturated compacted Boom clay, Eng. Geol., 54, 117–127, https://doi.org/10.1016/S0013-7952(99)00067-8, 1999.

Sadeghi, H. and AliPanahi, P.: Saturated hydraulic conductivity of problematic soils measured by a newly developed low-compliance triaxial permeameter, Eng. Geol., 278, 105827, https://doi.org/10.1016/j.enggeo.2020.105827, 2020.

Schrefler, B. A.: Mechanics and thermodynamics of saturated/unsaturated porous materials and quantitative solutions, Appl. Mech. Rev., 55, 351–388, 2002.

Shao, X., Zhang, H., and Tan, Y.: Collapse behavior and microstructural alteration of remolded loess under graded wetting tests, Eng. Geol., 233, 11–22, https://doi.org/10.1016/j.enggeo.2017.11.025, 2018.

Shepard, F. P.: Nomenclature based on sand-silt-clay ratios, J. Sediment. Res., 24, 151–158, https://doi.org/10.1306/d4269774-2b26-11d7-8648000102c1865d, 1954.

Skempton, A. W. and Brogan, J. M.: Experiments on piping in sandy gravels, Géotechnique, 44, 449–460, 1994.

Smalley, I.: Landslides in the thick loess terrain of North-West China, edited by Derbyshire, E., Meng, X., and Dijkstra, T. A., Eng. Geol., 59, 201–202, https://doi.org/10.1016/S0013-7952(00)00067-3, 2001.

Vallejo, L. E.: Interpretation of the limits in shear strength in binary granular mixtures, Can. Geotech. J., 38, 1097–1104, 2001.

van Genuchten, M. T.: A closed-form equation for predicting the hydraulic conductivity of unsaturated soils, Soil Sci. Soc. Am. J., 44, 892–898, https://doi.org/10.2136/sssaj1980.03615995004400050002x, 1980.

Wang, J.-D., Li, P., Ma, Y., and Vanapalli, S. K.: Evolution of pore-size distribution of intact loess and remolded loess due to consolidation, J. Soils Sediments, 19, 1226–1238, https://doi.org/10.1007/s11368-018-2136-7, 2019.

Watson, K. K.: An instantaneous profile method for determining the hydraulic conductivity of unsaturated porous materials, Water Resour. Res., 2, 709–715, https://doi.org/10.1029/WR002i004p00709, 1966.

Wu, F. C., Liu, Y., Zhao, X. N., and Guo, Z. T.: Research report on progress strategy of environmental science disciplines, Science Press, Beijing, 2021.

Xie, H., Chen, Z., and Wang, J.: Three-dimensional numerical analysis of deformation and failure during top coal caving, Int. J. Rock Mech. Min. Sci., 36, 651–658, 1999.

Ye, W., San, C., and Zhao, X.: Spatial-temporal distribution of loess and source of dust in Xinjiang, J. Desert Res., 23, 514–520, 2003 (in Chinese).

Zhang, Y. T.: Study on the influence of temperature on the permeability of remolded Malan loess, M.S. thesis, Chang'an University, Xi'an, China, 2019.

Zhuang, J. Q., Cui, P., Hu, K. H., and Chen, X. Q.: Fine particle size moving and its effect on debris flow initiation, Mt. Res. Dev., 33, 713–720, 2015a.

Zhuang, J. Q., Peng, J. B., Iqbal, J., Liu, T. M., Liu, N. N., Li, Y. Z., and Ma, P. H.: Identification of landslide spatial distribution and susceptibility assessment in relation to topography in the Xi'an region, Shaanxi Province, China, Front. Earth Sci., 9, 449–462, 2015b.